Pharm Res (2012) 29:2926–2935
DOI 10.1007/s11095-012-0799-0

RESEARCH PAPER

Powder Strength Distributions for Understanding De-agglomeration of Lactose Powders

Shyamal C. Das • Srinivas Ravindra Babu Behara • Jurgen B. Bulitta • David A. V. Morton • Ian Larson • Peter J. Stewart

Received: 19 December 2011 / Accepted: 31 May 2012 / Published online: 14 June 2012

ABSTRACT

Purpose The purpose was to calculate distributions of powder strength of a cohesive bed to explain the de-agglomeration of lactose.

Methods De-agglomeration profiles of Lactohale 300® (L300) and micronized lactose (ML) were constructed by particle sizing aerosolised plumes dispersed at air flow rates of 30–180 l/min. The work of cohesion distribution was determined by inverse gas chromatography. The primary particle size and tapped density distributions were determined. Powder strength distributions were calculated by Monte Carlo simulations from distributions of particle size, work of cohesion and tapped density measurements.

Results The powder strength distribution of L300 was broader than that of ML. Up to 85th percentile, powder strength of L300 was lower than ML which was consistent with the better de-agglomeration of L300 at low flow rates. However, ~15% of L300 particles had higher powder strength than ML which likely to cause lower de-agglomeration for L300 at high air flow rates.

Conclusion Cohesive lactose powders formed matrices of non-homogenous powder strength. De-agglomeration of cohesive powders has been shown to be related to powder strength. This study provided new insights into powder de-agglomeration by a new approach for calculating powder strength distributions to better understand complex de-agglomeration behaviour.

KEY WORDS de-agglomeration · dry powder inhaler · inverse gas chromatography · powder strength distribution · work of cohesion distribution

INTRODUCTION

Both active pharmaceutical ingredients (API) and ternary components such as lactose, commonly used in dry powder inhaler (DPI) formulations, are micron-sized and form cohesive matrices due to interparticulate interactions (1). In powder mixtures, these cohesive structures may be complex depending on the propensity of the cohesive-adhesive interactions of the materials (2). The de-agglomeration and aerosolization of these cohesive matrices are essential for effective delivery to the lower respiratory tract, the principal target of most respiratory drug delivery treatment (3). Although the target particle size of de-agglomerated powders is determined by the utilization purpose, it should be less than 5 μm for deposition in the lower respiratory tract (4). The factors influencing the complex de-agglomeration process have been a focus of research for better formulation design. One of the important factors that strongly influence

S. C. Das (✉) • S. R. B. Behara • D. A. V. Morton • I. Larson • P. J. Stewart
Drug Delivery, Disposition and Dynamics
Monash Institute of Pharmaceutical Sciences
Monash University (Parkville campus)
381 Royal Parade
Parkville, Victoria 3052, Australia
e-mail: shyamal.das@monash.edu

J. B. Bulitta
Centre for Medicine Use and Safety
Faculty of Pharmacy and Pharmaceutical Sciences
Monash University (Parkville campus)
Parkville, Australia

Present Address:
S. R. B. Behara
Department of Mechanical and Nuclear Engineering, School of Engineering
Virginia Commonwealth University
Richmond, Virginia, USA

the de-agglomeration and aerosolization processes is the tensile strength of the agglomerates (5). Tensile strength can be defined as the force per unit area of fracture that is necessary to split a powder compact (6). A number of models have been proposed to calculate tensile strength (6,8–10). One of the earliest models was that proposed by Rumpf (11):

$$\sigma = (1-\varepsilon).\left(\frac{k}{\pi}\right).\left(\frac{H}{d^2}\right) \quad \text{(i)}$$

where σ is the tensile strength of agglomerate, ε is the porosity of the aggregate, k is the coordination number (number of contacts per particle), H is the strength of interparticular bond and d is the particle diameter. This model formed the platform for further research on tensile strength calculation; however, it was based on the assumptions that all particles in the agglomerates are uniformly distributed mono-sized spheres, and the effective bonding bridges between particles fail simultaneously. Based on the Rumpf model, a number of modified equations for tensile strength calculation have been put forward over time which were documented by Schubert (7). One of the latest and widely accepted models was proposed by Kendall and Stainton (12):

$$\sigma = 15.6\left(\frac{\varphi^4 W}{d}\right) \quad \text{(ii)}$$

where, d is the particle diameter, φ is the packing fraction (volume of particles/volume of aggregates) and W is the work of adhesion or cohesion of particles.

De-agglomeration of powders, in general, decreases as the strength of agglomerates increases (5,13). An inverse relationship between dispersion and the strength of agglomerate has been reported for mannitol (14). However, the de-agglomeration of micronized pharmaceutical powders, studied by laser diffraction particle sizing of the aerosol cloud produced from commercial inhalation devices and shown by the percentage of particles less than 5.4 μm, fitted a sigmoidal function when the air flow rate (breaking force) was increased from 30 l/min to 180 l/min (15,16). The non-linear de-agglomeration behavior was attributed to a non-homogeneous powder-bed structure (where powder structure was considered to be a combination of the packing fraction, work of cohesion and particle size). The non-linear relationship of de-agglomeration profiles (15,16) has encouraged the authors of this paper to rethink about the de-agglomeration determining factors. In reality, cohesive powders consist of particles of varying size. Particle surfaces will have a distribution of surface energy (17) and therefore, the work of cohesion of powders is best represented by a distribution. The packing fraction will also vary across the powder bed. As all the three parameters, particle size, work of cohesion and packing fraction, have distributions in real interactive powder systems, it is hypothesized that the tensile strength of a powder will have a distribution, and the de-agglomeration will be related to tensile strength distributions rather than average values.

The purpose of this project was to test the hypothesis that the differing de-agglomeration behaviour of two micronized lactose powders can be explained by distribution of a tensile strength rather than average values. Using the equation of Kendall and Stainton (Eq. ii) above, the tensile strength distribution can be determined from the particle size distribution, the work of cohesion distribution and the packing fraction distribution. The determination of particle size distribution using laser diffraction is well established. The work of cohesion distribution, calculated from the surface energy distribution using inverse gas chromatography (17), is now possible using the van Oss concept (18). An experimental method for determination of packing fraction distribution in a cohesive powder bed is not available. In this study, the tapped density distribution (density of interactive powder bed at certain number of taps) was used in place of the packing fraction. From the distributions of particle size, work of cohesion and tapped density (ρ_t), a function of the tensile strength distribution which is termed as powder strength distribution in this paper (σ^*) was calculated using Monte Carlo simulation methodology and a slightly modified Eq. ii as follows:

$$\sigma^* = 15.6\left(\frac{\rho_t^4 W}{d}\right) \quad \text{(iii)}$$

The de-agglomeration-air flow rate profile of the lactose samples were explained using the powder strength distributions.

MATERIALS AND METHODS

Materials

Two lactose samples, Lactohale 300® (L300, Borculo Ingredients domo, Borculo, The Netherlands) and micronized lactose (ML) produced by micronization of α-lactose monohydrate (Lactose New Zealand, Hawera, New Zealand) using a fluid energy mill (K-tron Soder, NJ, USA) (5) were used.

Methods

Pre-processing of Powders

Powders were pre-processed before investigation according to a standardised hand mixing method developed in our lab and published previously (19). The mixing would ensure the powders to be exposed to similar mechanical processing. Each powder (5 g in each batch) was mixed in a jar for 5 min using three ceramic balls (10 mm diameter). After each 30 s mixing, the jar was tapped vertically and horizontally to loosen any

powder stuck to the jar wall. Primary particle size distributions (PSD) of lactose were compared before and after mixing. No significant difference in PSD was observed before and after mixing (result was not shown) indicating that size reduction was not happened as a result of this process.

Dispersion of Lactose in Air by Laser Diffraction

Accurately weighed 20±1 mg of powders were dispersed from gelatine no 3 capsules (Capsugel, NSW, Australia) through an inhalation cell of the laser diffraction instrument (Spraytec®, Malvern Instruments, Worcestershire, UK) horizontally for five seconds at 30, 45, 60, 90, 120, 150 and 180 l/min using a Rotahaler® (GSK, Middlesex, UK). The measurement was carried out, capturing 100 measurements per second over five seconds. Measurements were made on five replicates. The output provided a standard format of average scatter data together with concentration weighted average for the particles less than a specific size (15,16). The air flow rates used in this current investigation are realistic and are within the air flow rates of patients with respiratory disorders (50–400 l/min) (20–23). However, this manuscript reports on fundamental mechanistic study of the relative de-agglomeration of powders and the flow rates selected to provide an appropriate "relative de-agglomeration *versus* air flow rate" profile to characterise the de-agglomeration behaviour of the cohesive material.

Work of Cohesion Calculation by Determining Surface Energy Using Inverse Gas Chromatography

Surface energies were determined using an inverse gas chromatography (IGC, Surface Measurement Systems Ltd, and London, UK). Pre-silanised glass columns (300 mm×3 mm internal diameter) were packed with approximately 0.33 g of each powder and silanised glass wool was used to close both ends. All the columns were packed by tapping for four minutes using a tapping apparatus for powder packing (Surface Measurement System, London, UK). The powder filled columns were conditioned for 2 h at 303 K before each measurement to remove impurities from surface. All probes were carried into the column by helium run at a flow rate of 10 sccm (standard cubic centimetre per minute). The retention times were detected by a flame ionization detector, and the dead volume was calculated based on the elution time of methane which was run at a concentration of 0.1 p/p^0 (where p denotes the partial pressure and p^0 the vapour pressure).

Surface Energy Determination at Infinite Dilution

GC grade hexane, heptane, octane, nonane and decane (all from Sigma-Aldrich GmbH, Steinheim, Germany) for non-polar surface energy (γ^{NP}), and two polar probes (i.e., dichloromethane and ethyl acetate) for polar surface energy (γ^{P}) were used at a concentration of $0.03p/p^0$. The basic character (γ^-) of the surface was determined from the free energy of interaction of the monopolar acidic probe, dichloromethane and the acidic character was determined from the free energy of interaction with the monopolar basic probe, ethyl acetate (24). The γ^{P} was then calculated from the acidic and basic characters of surface using the van Oss concept (24,25). The total surface energy (γ^{T}) was the additive result of non-polar (γ^{NP}) and polar contributions (γ^{P}) (26). The work of cohesion (W) was calculated from surface energy values (18,27). The experiments were conducted in triplicate on the same batch.

Surface Energy and Work of Cohesion Distributions and Surface Area Determination at Finite Dilution

The non-polar surface energy distributions (γ^{NP} profile) were determined according to the method described elsewhere (28,29). The Brunauer-Emmet-Teller (BET) surface area was calculated from hexane adsorption isotherms. The surface coverage (n/n_m) was calculated from the adsorbed amount (n) and monolayer capacity (n_m, the number of moles of the probe adsorbed for monolayer coverage). At each surface coverage, the net retention volume (V_N) was calculated for each probe. The γ^{NP} was then calculated from the slope ($2\ N_A\ \sqrt{\gamma^{NP}}$) of a plot of $RTlnV_N$ against a $\sqrt{\gamma^{NP}}$ of alkanes (30). The γ^{P}, γ^{T} and W were calculated at each surface coverage and their profiles were constructed (17).

Tapped Density Distributions

The bulk density was measured by pouring the pre-processed powders slowly into a 10 ml measuring cylinder from a fixed height. The tapped density was determined after 1024 taps of an automatic tapper (AUTOTAP™, Quantachrome Instruments, Boynton Beach, FL, USA). The tapper was operated with a 3.18 mm vertical travel at a tapping speed of 260 taps/min. Four replicates of each sample were carried out. The Carr Index (31) was calculated from the bulk density and tapped density using the following Eq. iv:

$$Carr\ Index = \left(\frac{tapped\ density - bulk\ density}{tapped\ density}\right) \quad \text{(iv)}$$

Primary Particle Size Distributions

The primary particle size distributions of processed L300 and ML were determined by laser diffraction (Mastersizer®-S, Malvern Instruments, Worcestershire, UK) using 300RF lens equipped with 150 ml dispersion unit. Approximately 150 mg samples were sonicated in 5 ml dispersant (isopropyl alcohol)

for a specified time (5 min) prior to the measurement. An imaginary refractive index of 0.01 was used in this investigation. The mean particle size distribution of six replicates was characterized by the derived parameters (d_{10}, d_{50} and d_{90}).

Monte Carlo Simulations to Predict Powder Strength Distributions

Monte Carlo sampling methodology was employed to determine the powder tensile strength distribution shown in Eq. v below. The distributions for work of cohesion, packing fraction, and particle diameter were obtained experimentally. Cumulative probability distributions for these quantities were constructed by linear interpolation between the frequent measurements.

One random deviate each was drawn from the distribution of work of cohesion (W_i), tapped density (ρ_{ti}), and particle diameter (d_i). Powder strength (σ_i^*) was calculated from these three random deviates as (index i denotes the i^{th} random deviate):

$$\sigma_i^* = 15.6\left(\frac{\rho_{ti}^4 W_i}{d_i}\right) \quad \text{(v)}$$

In total, 1,000,000 random powder strength samples were calculated for each powder to obtain a distribution for powder strength of L300 and ML. These random samples for σ_i^* were utilized to calculate descriptive statistics such as the expectation value (arithmetic mean), standard deviation, and representative percentiles of powder strength to compare the L300 and ML powders. Perl scripts were developed to numerically implement these calculations and data processing. The Math random Perl package (version 0.71) was used to draw random deviates.

Statistical Modelling and Analysis

Dispersion data obtained from the laser diffraction instrument were modelled using a non-linear least square regression analysis in the SigmaPlot 9.0® software (Systat Software, Inc., IL, USA). The statistical significance was carried out using one-way analysis of variance with Tuckey's post-hoc analysis and between the groups was carried out using independent sample *t*-test using an alpha of 0.05 in SPSS (version 17.0, SPSS, Inc., IL, USA)

RESULTS

D-agglomeration of Lactose Powders

The relative de-agglomeration profiles of L300 and ML were obtained as shown elsewhere (16). Briefly, relative de-agglomeration was determined from the cumulative particle size of the aerosolised powder less than 5.4 μm (obtained from laser diffraction particle sizing of the aerosol plume) compared with the full availability of particles (measured by laser diffraction particle sizing of the powder in a liquid dispersant) in that size range. The relative de-agglomeration *versus* air flow rate profiles for both powders following aerosolization through the Rotahaler® are presented in Fig. 1. The relative de-agglomeration *versus* air flow rate profiles of the two lactoses showed two different profiles over the range of air flow rates used in this study (Fig. 1).

Both lactose samples showed an increase in relative de-agglomeration with increasing air flow rate. For L300, the relative de-agglomeration increased rapidly at low air flow rates but then began to level at 90 l/min with a relative de-agglomeration of about 30%. In contrast, the relative de-agglomeration of ML increased more slowly with increasing air flow rate reaching about 35% at 120 l/min. The relative de-agglomeration of L300 was significantly greater ($p<0.05$) than ML at air flow rates between 30 and 90 l/min (Fig. 1). For example, the relative de-agglomeration at 60 l/min was around 18% for L300 compared to 13% for ML.

The relative de-agglomeration of ML was not significantly different between 120 and 180 l/min ($p>0.05$) whereas the relative de-agglomeration of L300 also was not significantly different between 90 and 180 l/min ($p>0.05$). At flow rates greater than 120 l/min, although the relative de-agglomeration of ML was higher than L300, the de-agglomeration was only significantly different at 150 l/min ($p<0.05$).

The data of de-agglomeration profiles were empirically modelled by a nonlinear least squares (32) regression using SigmaPlot 9.0 software using sigmoid 3-parameter model (Eq. vi). This approach has been used in previous studies to allow the estimation of the sigmoidal equation parameter ('*a*' and '*b*' and *x*0) which characterized the aerosolization

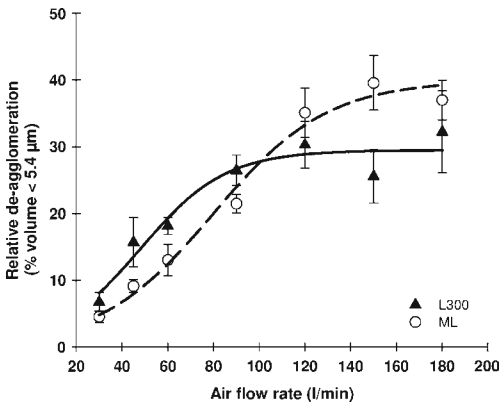

Fig. 1 The relative de-agglomeration profile of percent of particles less than 5.4 μm *versus* air flow rate for the aerosolised plume of Lactohale 300 (L300) and micronized lactose (ML) from Rotahaler determined by laser diffraction ($n=5$).

behaviour of the powders. The requirements for determining the best fit have been described previously (33).

$$y = \frac{a}{1 + e^{-\left(\frac{x-x0}{b}\right)}} \quad \text{(vi)}$$

where, '*a*'and '*b*' represent the maximum extent of relative de-agglomeration of the powder and the change in relative de-agglomeration with air flow rate, respectively. The parameter '*x*0' is the air flow rate required to achieve 50% relative de-agglomeration. The estimated parameters for L300 and ML using sigmoid 3-parameter fitting are shown in Table I. The estimated maximum relative de-agglomeration for ML of 40% was higher than that for L300 which was 29.5%. These estimated parameters were consistent with the experimental de-agglomeration *versus* air flow rate profiles for the two lactose samples. Also, the other estimated parameters of change in relative de-agglomeration ('*b*') with air flow rate and the air flow rate required to achieve 50% relative de-agglomeration (*x*0) were different for the two lactose samples. It was not possible to test the significance of these differences due to the need to use all replicates of relative de-agglomeration in the one modelling event in order to have sufficient data to estimate meaningful parameters. The data presented here in the relative de-agglomeration profile and modelling show clearly that the two lactose samples behave quite differently in their de-agglomeration characteristics.

Surface Energy

Surface Energies at Infinite Dilution

The non-polar, polar and total surface energies at infinite dilution are shown in Fig. 2. No significant difference in non-polar surface energy was observed between L300 (46.9± 0.4 mJ/m^2) and ML (46.0±0.4 mJ/m^2) ($p>0.05$). The polar surface energy of L300 was significantly lower than that of ML ($P<0.05$) which resulted in the total surface energy of L300 being significantly lower than ML ($p<0.05$). The polar surface energy calculation was based on the van Oss acidic and basic numbers of dichloromethane and ethyl acetate. In the calculation, the acidity value of dichloromethane was used as 5.20 mJ/m^2 and the basicity value for ethyl acetate was used as 19.20 mJ/m^2 (Surface Measurement Systems). However, in the literature different values are available for each solvent (17,34). If the other values of acidity of dichloromethane and basicity of ethyl acetate are used, the ultimate basic and acidic property of lactose samples would change resulting in the change in polar energy and total energy. Moreover, these two probes were considered monopolar although dichloromethane has little basicity and ethyl acetate has little acidity values. Therefore, the accuracy of the ultimate polar and total surface energy values depends on these input parameters. The polar and total surface energy showed similar values to those found in other studies (24,25). The surface energy at infinite dilution provided the surface energy of the most energetic sites and was used in the surface energy distributions.

Table I Nonlinear Least Squares Estimated Parameters of a, b and x0 for the 3-parameter Fitting of the Relative De-agglomeration *Versus* Flow Rate Profile for Lactohale 300 (L300) and Micronized Lactose (ML)

Material	*a*	*b*	*x*0
L300	29.48	18.60	48.01
ML	39.97	25.10	79.84

Surface Energy at Finite Dilution

The non-polar, polar and total surface energy distributions determined at finite dilution using IGC are shown in Fig. 3. The surface coverages of this experiment were different for these two lactoses, and the maximum surface coverage was just under 6%. The maximum surface coverage is determined by the surface area of the material and the retention volumes of probes where no intermolecular interactions between probe molecules take place. The surface coverage is calculated by dividing the adsorbed amount by monolayer capacity of solvent. The monolayer surface coverage for small lactose is higher than monolayer surface coverage for coarse lactose as the monolayer capacity is calculated by dividing surface area of the material by the surface area of the solvent. Therefore, a greater surface coverage can be achieved for coarse lactose than small lactose. To authors' experience, 20–25% surface coverage was obtained for coarse lactose whereas only around 5% surface coverage was obtained for micronized lactose (34). The non-polar surface energy (Fig. 3a) of L300 was higher than that of ML over the surface coverage of about 4 %. However, the polar surface energy of L300 was lower than ML over the surface coverage of 3% (Fig. 3b). Similarly, the total surface energy of L300 was lower than ML over surface

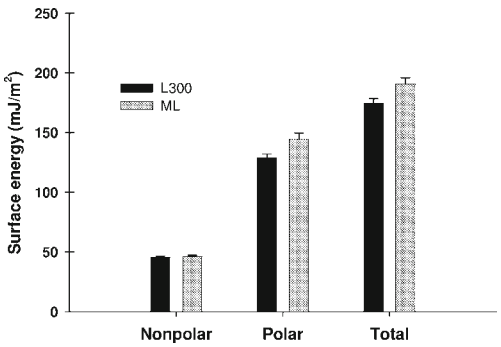

Fig. 2 Non-polar, polar and total surface energies of Lactohale 300 (L300) and micronized lactose (ML) determined by inverse gas chromatography at infinite dilution.

coverage of 3% (Fig. 3c). The limitations of surface energy distribution measurement have been discussed previously (17,29). In addition, the surface energy was determined based on the interaction of probes with surface sites. The infinite dilution measurement was developed to maintain an environment so that no competition occurred among adsorbate molecules for interaction with the adsorbent surface sites. In finite dilution, the adsorbate concentration was increased to finite dilution range leading to increased concentration of molecules on the surface sites. There was a possibility of interactions among adsorbent molecules that might change retention volumes. Therefore, careful attention was given in accepting the retention volumes of probes at finite dilution. Retention volumes would be expected to decrease with increasing adsorbate concentration; however, where deviations were found in this trend, those data were not accepted. Moreover, in the calculation of surface energy, only the surface energy values with $r^2 \geq 0.999$ were accepted.

Work of Cohesion

The work of cohesion of L300 was lower than that of ML up to approximately 3% of surface coverage (Fig. 4a). The work of cohesion approached a constant value of around 186 mJ/m^2 at surface coverages of 3.18% for L300 and of 5.19% for ML. For powder strength distribution calculation, the data were rearranged as the per cent surface coverage *versus* work of cohesion (Fig. 4b).

Particle Size by Liquid Dispersion in Laser Diffraction

The cumulative undersize *versus* particle size distributions are shown in Fig. 5. The volume mean diameter of ML (2.8± 0.1 μm) was significantly lower than that of L300 (4.1± 0.1 μm) ($p<0.05$). Little difference was observed between two lactoses for the smaller size particles and this is shown by the fact that there was no significant difference in the d_{10} of the distributions of both powders (i.e. d_{10} for L300 and ML were 0.2±0.1 μm and 0.3±0.1 μm, respectively ($p>0.05$). However, the distribution does diverge at the larger particle sizes with the d_{90} being significantly different (i.e. d_{90} for L300 and ML were 9.1±0.1 μm and 6.7±0.3 μm, respectively ($p<$ 0.05). No particles were greater than 21 μm for both L300 and ML.

Tapped Density and Other Bulk Properties

No significant difference ($p>0.05$) was observed in bulk properties such as bulk density and Carr Index between the two powders (Table II). However, the tapped density was significantly different ($p<0.05$). Therefore, the tapped density *versus* number of taps profile of the two powders was compared over 1024 taps.

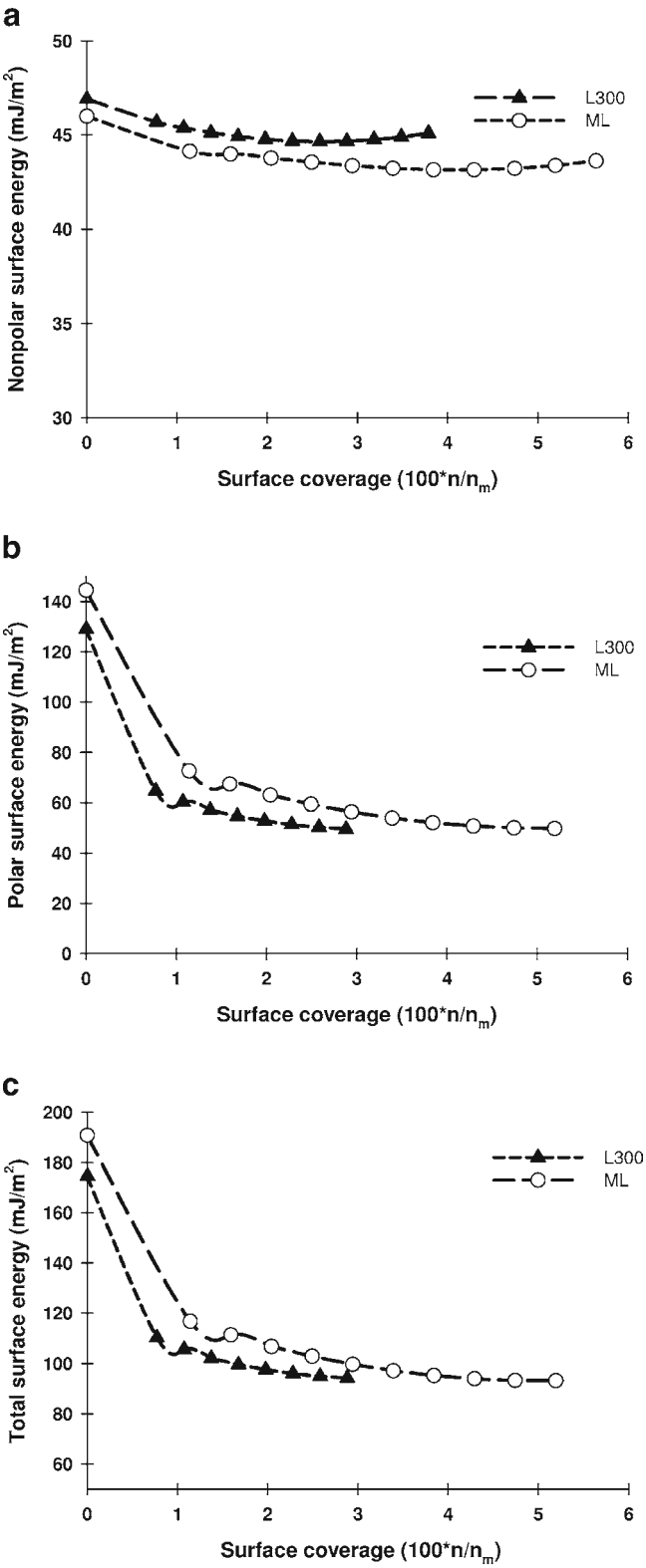

Fig. 3 (**a**) Non-polar, (**b**) polar, (**c**) total surface energy distributions of Lactohale 300 (L300) and micronized lactose (ML) determined by inverse gas chromatography at finite dilution.

The tapped density *versus* number of taps profile provided an indication of the packing fraction distribution of both

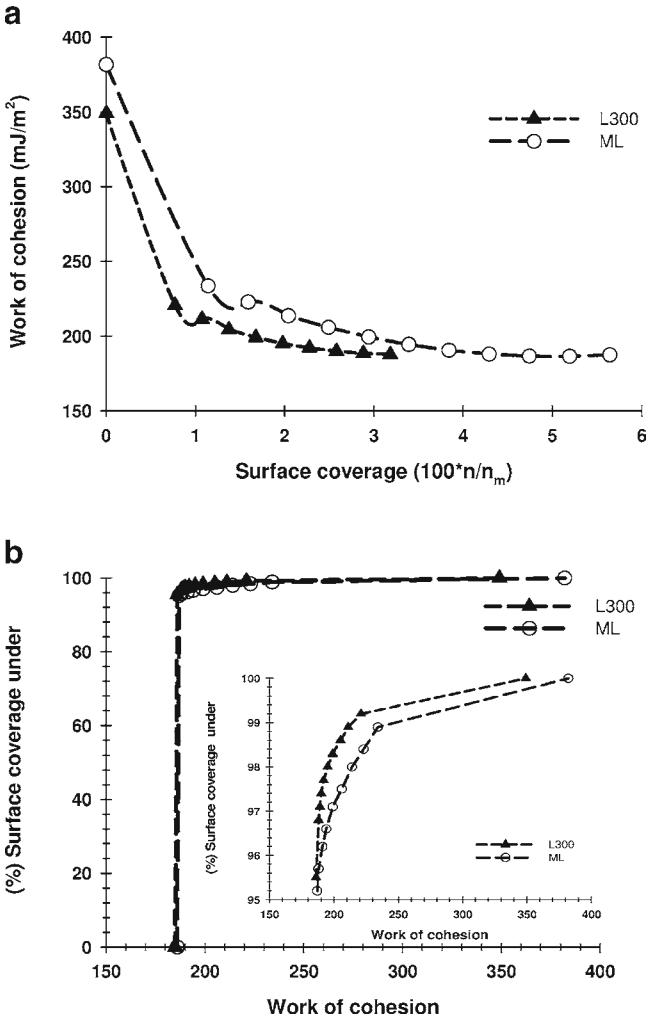

Fig. 4 (**a**) Work of cohesion distribution at different surface coverage. (**b**) Cumulative probability distributions of work of cohesion of Lactohale 300 (L300) and micronized lactose (ML) determined by inverse gas chromatography at finite dilution (the difference in work of cohesion was shown in the inset).

powders. Tapped density is measured as weight per volume of powder and numerically is similar to packing fraction. It is difficult to experimentally measure packing fraction across small sections of a powder bed in order to determine a distribution. In this case, the distribution was determined by measuring the change in tapped density with number of standard taps. Micro-areas of a powder bed having a greater packing fraction will consolidate to a greater extent during the tapping process, and vice versa. For these powders, the bulk properties of the two lactose samples, shown by the bulk density and Carr Index are not different. However, the powders behaved differently to consolidation processes revealing that the structure of the powders was different.

Table II Bulk Properties of Lactohale 300 (L300) and Micronized Lactose (ML)

	L300	ML	p-value
Bulk density (g/ml)	0.279 ± 0.009	0.274 ± 0.021	0.666
Tapped density (g/ml)	0.518 ± 0.010	0.484 ± 0.020	0.020
Carr index	0.462 ± 0.013	0.435 ± 0.024	0.094

The tapped density *versus* number of taps profile has been converted to a cumulative distribution and the difference in behaviour of the lactose samples is seen in Fig. 6. The tapped density was not significantly different up to around 10% relative taps. However, as the number of taps was increased, the tapped density of L300 was increasingly higher than ML.

Powder Strength Distribution (σ*)

The distribution of the powder strength (σ*) was notably wider for L300 compared to ML (Fig. 7).

Both L300 and ML had similar arithmetic means, but the variance was approximately 2.0 fold larger for L300 compared to ML (Table III). Percentiles were used as a nonparametric representation of the powder strength distribution. Up to the 85% percentile, every percentile was lower for L300

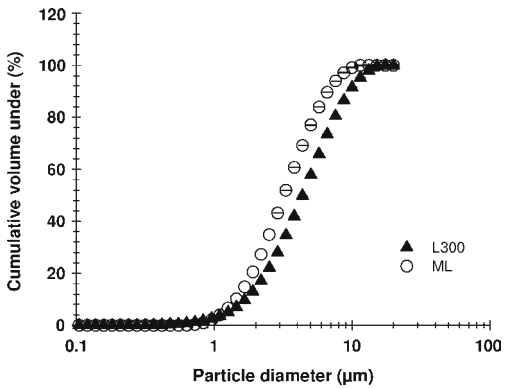

Fig. 5 Cumulative particle size distribution (PSD) of lactoses (L300 and ML) determined by laser diffraction in liquid medium (n=5, data represents mean ± standard deviation).

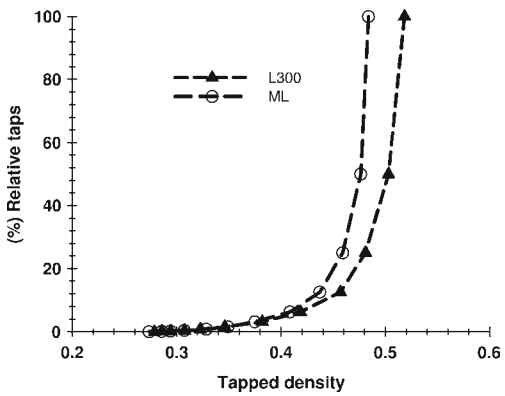

Fig. 6 Cumulative probability distributions of tapped density of lactoses (L300 and ML) (n=4, data represents mean ± standard deviation).

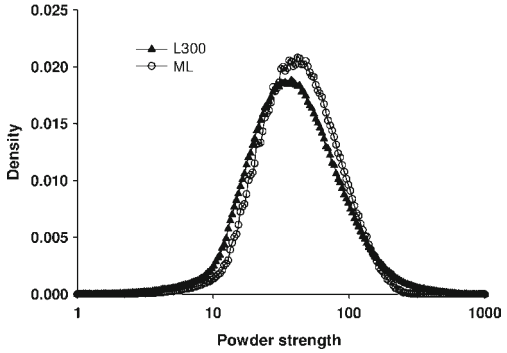

Fig. 7 Powder strength (σ*) distribution of Lactohale 300 (L300) and micronized lactose (ML) determined from cumulative work of cohesion distribution (Fig. 4b), particle size distribution (Fig. 5) and tapped density distribution (Fig. 6) by Monte Carlo simulation.

compared to ML (Table III). However, the 95% and 99.5% percentile was notably higher for L300 compared to ML. The powder strength distribution of L300 had a 99% nonparametric interval (0.5 to 99.5% percentile) from 4.47 to 326, whereas this interval for ML was from 6.39 to 196 (Table III).

DISCUSSION

The purpose of this research was to test the hypothesis that the de-agglomeration behaviour can be better explained by the powder strength of the cohesive lactose samples. The de-agglomeration and aerosolization behaviours of the two micronized powders (L300 and ML) were different as shown in Fig. 1. The properties of the powder bed that affect de-agglomeration (particle size, work of cohesion and density) were different between both powders (Figs. 2, 3, 4, 5, and 6 and Tables I and II). However, neither of these three properties alone could explain the behaviour of the two lactoses. While the increased de-agglomeration of L300 over ML at air flow rates between 30 and 90 l/min could be explained by the slightly larger size and lower work of cohesion of L300, this explanation did not hold for de-agglomeration behaviour at higher air flow rate over 90 l/min.

The cohesive lactose samples were considered to be an interacting matrix which possessed a distribution of particles size, tapped density and work of cohesion. Using the equation of Kendall and Stainton (12) and the distributions of particle size, tapped density and work of cohesion, a distribution of the powder strength was determined for the two lactose samples (Fig. 7). The estimated strength distributions of the two lactoses were different.

L300 had a broader distribution of powder strength and possessed both lower and higher powder strengths than ML. This was consistent with the de-agglomeration behaviour where L300 showed a greater propensity to de-agglomerate at low air flow rates (and low energies) because the powder contained cohesive structures which were less strong than ML. In contrast, at high flow rates, L300 possessed cohesive structures of higher powder strength than ML. In fact, the powder strengths were so high that L300 failed to de-agglomerate further after an air flow rate of 90 l/min.

While the present study proposes the, to our knowledge, first approach to calculate the distribution of tensile strength by Monte Carlo simulation methodology, it is important to discuss the assumptions of this approach. In this study, the powder strength was calculated from particle size distribution, work of cohesion distribution and tapped density distribution using Kendall and Stainton equation (12) by Monte Carlo simulations. This calculation of the distribution was based on several assumptions. Firstly, the work of cohesion of the two lactoses will be similar and constant over the remaining surfaces beyond approximately 3.0% for L300 and 5.0% for ML. The surface energy and thus work of cohesion could not be determined beyond 3.18% for L300 and 5.19% for ML since the retention volume started to decrease as the concentration of the probe was increased beyond this concentration. The assumption of similar and constant surface energy was a reasonable one as the surface energy of several pharmaceutical powders has been found to reach constant values at higher surface coverage in previous studies (33,35). This means that the heterogeneity of surface energy (and thus work of cohesion) of the L300 and ML was associated with the higher energy differences for only a small area of the surface. The distribution of the packing fraction of Kendall and Stainton equation (12) was replaced by tapped density distribution during this calculation. Additional studies are necessary to further support these assumptions and potentially refine the proposed computational approach.

CONCLUSIONS

The cohesive lactose samples formed interacting matrices of non-homogenous powder strength. The distributions of the key de-agglomerating properties of two cohesive lactose samples were determined, including particle size, tapped density and work of cohesion. The differing de-agglomeration and aerosolization behaviour of the two lactose powders was

Table III Powder Strength Distributions for Lactohale 300 (L300) and Micronized Lactose (ML) Based on 1,000,000 Monte Carlo Samples

Sample	Average	Variance	0.5%	5%	25%	50%	75%	85%	95%	99.5%
L 300	52.6	2502	4.47	12.2	23.5	38.0	63.5	84.7	140	326
ML	51.8	1237	6.39	14.9	27.1	42.1	66.2	84.2	123	196

explained by the differing distributions of powder strength calculated based on Kendall and Stainton (12) tensile strength equation using Monte Carlo simulations. The study demonstrated the advantages of using the distributions of key controlling parameters to calculate the powder strength distribution in order to explain the de-agglomeration behaviour. This Monte Carlo approach seems preferable, since it does not require the use of average values.

The study's limitations and assumptions include the use of tapped density distributions to represent packing fraction, the inherent limitations of inverse gas chromatography in determining surface energy at finite dilution and the extrapolation of work of cohesion data to determine the full surface energy distributions.

The methodology needs to be extended to other cohesive powders to confirm its application in a more general sense. However, it does provide a valuable approach to better understand de-agglomeration behaviour of cohesive powders by calculation of distributions for powder strength.

ACKNOWLEDGMENTS AND DISCLOSURES

Srinivas Ravindra Babu Behara (SRBB) is a recipient of Monash International Postgraduate Research Scholarship and Monash Research Graduate Scholarship. The authors would like to thank BorculoIngredientsDomo for providing lactohale 300 powder.

REFERENCES

1. Jones MD, Price R. The influence of fine excipient particles on the performance of carrier-based dry powder inhalation formulations. Pharm Res. 2006;23:1665–74.
2. Louey M, Stewart P. Particle interactions involved in aerosol dispersion of ternary interactive mixtures. Pharm Res. 2002; 19:1524–31.
3. Xu Z, Mansour H, Hickey A. Particle interactions in dry powder inhaler unit processes: a review. J Adh Sci Technol. 2011;25:451–82.
4. Qui Y, Adjei AL, Gupta PK. Absorption and bioavailability of inhaled peptides and proteins. In: Adjei AL, Gupta PK, editors. Inhalation delivery of therapeutic peptides and proteins. New York: Marcel Dekker, Inc.; 1997.
5. Adi H, Larson I, Chiou H, Young P, Traini D, Stewart P. Agglomerate strength and dispersion of salmeterol xinafoate from powder mixtures for inhalation. Pharm Res. 2006;23:2556–65.
6. Cheng D. The tensile strength of powders. Chem Eng Sci. 1968;23:1405–20.
7. Schubert H. Tensile strength of agglomerates. Powder Technol. 1975;11:107–19.
8. Ashton M, Cheng D, Farley R, Valentin F. Some investigations into the strength and flow properties of powders. Rheologica Acta. 1965;4:206–18.
9. Kocovaand S, Pilpel N. The tensile strength of mixtures of cohesive powders. Powder Technol. 1973;7:51–67.
10. Shinoharaand K, Tanaka T. 3rd International Congress. Marianske Lazne: CHISA; 1969.
11. Rumpf H. The strength of granules and agglomerates. In: Knepper WA, editor. International symposium on agglomeration 1st. New York: Interscience; 1962. p. 379–418.
12. Kendall K, Stainton C. Adhesion and aggregation of fine particles. Powder Technol. 2001;121:223–9.
13. Das S, Larson I, Young P, Stewart P. Influence of storage relative humidity on the dispersion of salmeterol xinafoate powders for inhalation. J Pharm Sci. 2009;98:1015–27.
14. Adi S, Adi H, Chan H, Finlay W, Tong Z, Yang R, Yu A. Agglomerate strength and dispersion of pharmaceutical powders. J Aerosol Sci. 2011;42:285–94.
15. Behara SRB, Kippax P, McIntosh MP, Morton DAV, Larson I, Stewart P. Structural influence of cohesive mixtures of salbutamol sulphate and lactose on aerosolisation and de-agglomeration behaviour under dynamic conditions. Eur J Pharm Sci. 2011;42:210–9.
16. Behara SRB, Larson I, Kippax P, Morton DAV, Stewart P. An approach to characterising the cohesive behaviour of powders using a flow titration aerosolisation based methodology. Chem Eng Sci. 2011;66:1640–8.
17. Das SC, Larson I, Morton DAV, Stewart PJ. Determination of the Polar and Total Surface Energy Distributions of Particulates by Inverse Gas Chromatography. Langmuir. 2011;27:521–3.
18. Vanoss CJ, Good RJ, Chaudhury MK. Additive and nonadditive surface-tension components and the interpretation of contact angles. Langmuir. 1988;4:884–91.
19. Alway B, Sangchantra R, Stewart PJ. Modelling the dissolution of diazepam in lactose interactive mixtures. Int J Pharm. 1996; 130:213–24.
20. Behara SRB, Larson I, Kippax P, Morton DAV, Stewart P. Insight into pressure drop efficiencies of dry powder inhalers. Eur J Pharm Sci. 2012;46:142–8.
21. Coady TJ, Davies HJ, Barnes P. Evaluation of a breath actuated pressurized aerosol. Clin Allergy. 1976;6:1–6.
22. Sarinas PSA, Robinson TE, Clark AR, Canfield J, Chitkara RK, Fick RB. Inspiratory flow rate and dynamic lung function in cystic fibrosis and chronic obstructive lung diseases. Chest. 1998; 114:988–92.
23. Wijkstra PJ, Vandermark TW, Boezen M, Vanaltena R, Postma DS, Koeter GH. Peak inspiratory mouth pressure in healthy-subjects and in patients with COPD. Chest. 1995;107:652–6.
24. Thielmann F, Naderi M, Burnett D, Jervis H. Investigation of the acid-base properties of an MCM-supported ruthenium oxide catalyst by inverse gas chromatography and dynamic vapour sorption. Jackson, SD, Hargreaves, JSJ, Lennon, D, (Eds.), Catalysis in application: Great Britain, Royal Soc. Chem. 2003;237.
25. Traini D, Young PM, Thielmann F, Acharya M. The influence of lactose pseudopolymorphic form on salbutamol sulfate-lactose interactions in DPI formulations. Drug Dev Ind Pharm. 2008; 34:992–1001.
26. Grimsey IM, Feeley JC, York P. Analysis of the surface energy of pharmaceutical powders by inverse gas chromatography. J Pharm Sci. 2002;91:571–83.
27. Tay T, Das S, Stewart P. Magnesium stearate increases salbutamol sulphate dispersion: what is the mechanism? Int J Pharm. 2010;383:62–9.
28. Thielmann F, Burnett DJ, Heng JYY. Determination of the surface energy distributions of different processed lactose. Drug Dev Ind Pharm. 2007;33:1240–53.
29. Yla-Maihaniemi PP, Heng JYY, Thielmann F, Williams DR. Inverse gas chromatographic method for measuring the dispersive surface energy distribution for particulates. Langmuir. 2008; 24:9551–7.
30. Schultz J, Lavielle L, Martin C. The role of the interface in carbon-fiber epoxy composites. J Adh. 1987;23:45–60.
31. Carr RL. Evaluating flow properties of solids. Chem Eng. 1965;72:163–8.

32. Marquardt D. An algorithm for least-squares estimation of nonlinear parameters. J So Ind Appl Math. 1963;11:431–41.
33. Draper N, Smith H. Applied regression analysis. New York: Willey; 1981.
34. Das S, Zhou Q, Morton D, Larson I, Stewart P. Use of surface energy distributions by inverse gas chromatography to understand mechanofusion processing and functionality of lactose coated with magnesium stearate. Eur J Pharm Sci. 2011;43:325–33.
35. Ho R, Hinder SJ, Watts JF, Dilworth SE, Williams DR, Heng JYY. Determination of surface heterogeneity of D-mannitol by sessile drop contact angle and finite concentration inverse gas chromatography. Int J Pharm. 2010;387:79–86.